

Article

Phosphate Adsorption onto an Al-Ti Bimetal Oxide Composite in Neutral Aqueous Solution: Performance and Thermodynamics

Xuefeng Wei ^{1,2,*}, Juan Miao ¹, Zhen Lv ¹, Xiaoyang Wan ¹, Ning Zhang ¹, Ruichang Zhang ^{1,2,*} and Shuge Peng ^{1,2,*}

¹ College of Chemical Engineering & Pharmaceutics, Henan University of Science and Technology, Luoyang 471023, China; miaojuan@haust.edu.cn (J.M.); 181408040216@stu.haust.edu.cn (Z.L.); 15737195097@163.com (X.W.); 9906114@haust.edu.cn (N.Z.)

² Provincial and Ministerial Co-Construction of Collaborative Innovation Center for Non-Ferrous Metal New Materials and Advanced Processing Technology, Luoyang 471023, China

* Correspondence: xfwei@haust.edu.cn (X.W.); ruichangzhang@126.com (R.Z.); sgpeng@haust.edu.cn (S.P.); Tel.: +86-379-64231914 (X.W.); Fax: +86-379-65627502 (X.W.)

Abstract: Phosphorus (P) pollution and phosphorus recovery are important issues in the field of environmental science. In this work, a novel Al-Ti bimetal composite sorbent was developed via a cost-effective co-precipitation approach for P removal from water. The adsorptive performance and characteristics of P onto Al-Ti sorbent were evaluated by batch adsorption experiments. The effects of Al:Ti molar ratio, initial P concentration and reaction temperature were investigated. The microstructural characteristics of the Al-Ti sorbent were confirmed by scanning electron microscopy (SEM), X-ray diffraction (XRD) analysis, Fourier transform infrared (FTIR) spectroscopy, and nitrogen adsorption-desorption measurements. Kinetic studies showed that the adsorption of P on Al-Ti oxide proceeds according to pseudo-second-order kinetics. The maximum adsorption capacity of phosphate on the Al-Ti oxide calculated from linear Langmuir models was 68.2 mg-P/g at pH 6.8. The Al-Ti oxide composite sorbent showed good potential for P recovery, owing to its large adsorption capacity and ease of regeneration.

Keywords: Al-Ti bimetal oxide; phosphate; adsorption; isotherm models; water treatment



Citation: Wei, X.; Miao, J.; Lv, Z.; Wan, X.; Zhang, N.; Zhang, R.; Peng, S. Phosphate Adsorption onto an Al-Ti Bimetal Oxide Composite in Neutral Aqueous Solution: Performance and Thermodynamics. *Appl. Sci.* **2022**, *12*, 2309. <https://doi.org/10.3390/app12052309>

Academic Editors: Ning Li, Xiuwen Cheng and Yanbiao Liu

Received: 9 December 2021

Accepted: 17 February 2022

Published: 23 February 2022

Publisher's Note: MDPI stays neutral with regard to jurisdictional claims in published maps and institutional affiliations.



Copyright: © 2022 by the authors. Licensee MDPI, Basel, Switzerland. This article is an open access article distributed under the terms and conditions of the Creative Commons Attribution (CC BY) license (<https://creativecommons.org/licenses/by/4.0/>).

1. Introduction

Phosphorus (P) is a vital macronutrient that promotes the growth and development of living organisms. The rapidly burgeoning human population has led to a rising demand for high agricultural and industrial productivity, which, inevitably, has led to an exponential increase in the consumption of fertilizer and detergent. Since P is present in several minerals and rocks, it is a fundamentally non-renewable resource. Unfortunately, the most accessible high-grade P in rocks and minerals is being exhausted. Over the next 50–100 years, P in rock reserves worldwide are expected to become depleted [1].

On the other hand, pernicious eutrophication and algae bloom of receiving waters, such as rivers, reservoirs, lakes, and coastal waters have become worldwide environmental problems, characterized by the rapid growth of cyanobacteria and algae that consume a considerable amount of dissolved oxygen and cause the subsequent death of aquatic life [2]. The consequences of these processes are the disruption of the ecological balance in water ecosystems and the deterioration of freshwater quality [3]. The excessive discharge of P into aquatic ecosystems results in these problems. Eutrophication leads to fish death and habitat degradation with the loss of plant and animal species [4]. Rapid decomposition of dense algae scum can give rise to foul odors and promote the growth of blue-green algae, which produce extensive toxic blooms [5,6]. Eutrophication can also promote parasitic

infections and amphibian diseases [7]. Recent reports suggest that phosphorus reduction effectively controls eutrophication [8,9]. Stringent legislation to curb P emissions has been established in many countries. In China, the discharge limit of P recommended for wastewater treatment plants is 0.5 mg/L for class 1 (as total P) [10]. Thus, there is an urgent demand for ways to recover P, as well as to decrease P-rich effluent to below threshold values to protect water bodies from eutrophication.

Diverse techniques have been applied to remove P from effluent, including physical, chemical, and biological processes. Although chemical methods such as precipitation [11] and coagulation [12] are relatively efficient for P removal, the disposal of accumulated sludge and secondary pollution caused by high chemical consumption are the main disadvantages of chemical methods [3]. As an alternative, biological treatment is considered feasible for P removal [13]. As they rely on phosphorus-accumulating bacteria, such systems are quite sensitive to water properties such as temperature and pH. Therefore, these systems are less stable and reliable, complex, and occupy a large area, which restricts the development of biological methods. Furthermore, electro dialysis does not satisfy the discharge requirements for effluent quality and requires post-treatment [14]. Currently, the sorption approach has shown great potential for P removal from contaminated water. Its advantages include low power consumption, low operating cost, convenient operation [15].

Therefore, the key issue is to find efficient adsorbents. Numerous natural and synthetic adsorbents, such as dolomite [16], clay minerals [17], orange waste [18], graphene [19], metal oxides [20], and activated alumina [21] have been introduced as alternatives for lowering P levels in aqueous solution. It has been reported that P has a relatively strong affinity for mineral surfaces [21]. Among these adsorbents, metal oxides (including hydroxides and oxyhydroxides), such as iron (hydr) oxides, are gaining popularity, owing to their high selectivity toward P. P can strongly adsorb onto the surface of metal oxides, especially iron and aluminum oxides rich in soils and sediments, including hematite (α -Fe₂O₃), magnetite (Fe₃O₄), maghemite (γ -Fe₂O₃), goethite (α -FeOOH), gibbsite (α -Al(OH)₃), boehmite (γ -AlOOH), and ferrihydrite (δ -FeOOH) [22–24]. Anion complexing capacity is an important factor responsible for the affinity of P for metal oxide surfaces, which allows binding to surface groups by ligand exchange reactions [25]. The sorption of P on iron/aluminum oxide-based composite sorbents containing two (or more) metal oxides has been reported in the literature. Such adsorbents, e.g., Al-Fe oxide [26], Fe-Mn oxide [27], Fe-Cu oxides [20], Mg-Al hydroxides, and Mg-Fe hydroxides [28], have been reported for P removal and are mostly comprised of divalent and trivalent cations. It has also been reported that composite metal oxides not only retain the advantages of single component oxides but can also significantly improve their sorption capacity.

Titanium (Ti) is one of the primary elements in the environment, similar to iron and aluminum. Recent reports demonstrate that titanium (IV) is a new alternative material exhibiting an acceptable sorption capacity for P [29]. Therefore, it can be expected that if Ti salts are incorporated into aluminum or iron oxides, the resulting product will not only retain the favorable properties of their individual components but also display enhanced capacity for P sorption owing to a synergistic effect. Mixed metal oxides, with Ti introduced, designed with multivalent metal ions, particularly tetravalent cations (Ti⁴⁺), could form more sorption sites (\equiv M-OH) and reactive surfaces if defects are created [30]. Fe-Ti oxides have been synthesized and exhibit the potential to be sorbents for P removal [31]. However, to the best of our knowledge, there has been no report on P adsorption by Al-Ti oxides.

In the present study, a series of Al-Ti bimetal oxides with different Al/Ti molar ratios was synthesized via a co-precipitation method and tested for P sorption from aqueous solutions, to determine the optimum Al/Ti molar ratio in bimetal oxides. The morphological structure and adsorption properties of the Al-Ti bimetal oxides were examined by X-ray diffraction (XRD), scanning electron microscopy (SEM), Fourier transform infrared (FTIR) spectroscopy, and nitrogen adsorption-desorption measurements. Measurements of adsorption isotherms and thermodynamics were carried out to explore the adsorption process. In addition, regeneration and recovery of used Al-Ti oxides were performed by their exposure to

alkaline solution and subsequent filtration with water. The purpose of this study is as follows: (i) to verify whether a new bimetallic Al-Ti oxides can adsorb phosphorus; (ii) evaluate the effects Al/Ti molar ratios, initial P concentration on the adsorption; (iii) determine the adsorption isotherm.

2. Materials and Methods

2.1. Synthesis of Al-Ti Oxide

Al-Ti oxide was prepared by a co-precipitation procedure. In brief, analytical-grade $\text{Al}_2(\text{SO}_4)_3 \cdot 8\text{H}_2\text{O}$ ($\geq 99.0\%$, Tianjin Chemical Reagent Co., Ltd., China) and $\text{Ti}(\text{SO}_4)_2$ ($\geq 96.0\%$, Beijing, Sinopharm Chemical Reagent Co., Ltd., China) with 1 mol/L total metal concentration were dissolved in 200 mL of deionized water. The solutions had Al(III):Ti(IV) molar ratios of 1:0, 4:1, 2:1, 1:1, 1:2, 1:4, and 0:1. In this case, ammonia water (12.5%) was slowly dripped into 200 mL of metal solutions with a predetermined amount of aluminum (III) sulfate and titanium (IV) sulfate until a pH of 7.5 was obtained. Then, the mixture was stirred constantly for 1 h and aged statically for 4 h at room temperature. The mixture was filtered and washed with anhydrous alcohol repeatedly. The materials were subsequently dried at 373 K, ground into fine powder, and then stored in a desiccator before use.

2.2. Characterization

The surface morphology and elemental composition of synthesized Al-Ti oxide were obtained using an SEM (Hitachi Limited, SU8020, Tokyo, Japan) instrument at 3.0 kV. Infrared absorption spectra analyses were performed with an FTIR (Shimadzu Trace 100) spectrometer in the $500\text{--}4000\text{ cm}^{-1}$ range. Attenuated total reflection with germanium crystals (ATR Top-Plate) was used. Absorbance measurements were performed using software provided by Omnic 32. The XRD was performed using an X-ray diffractometer (D8 ADVANCE, Bruker, Germany) with Cu-K α radiation ($\lambda = 1.5406\text{ \AA}$), tube current of 40 mA, and tube voltage of 40 kV. N_2 adsorption-desorption isotherms were measured at 77 K with a surface area analyzer (Micromeritics ASAP 2460, Norcross, GA, USA). The pretreatment was conducted at 473 K for 6 h. The Brunauer–Emmett–Teller equation and Barrett–Joyner–Halenda method were used to calculate the surface area and pore size of Al-Ti oxide. The ζ -potential was measured by Zetasizer Nano series (Nano ZS, Malvern, England).

2.3. Batch Experiments

The adsorption tests were conducted at different initial P concentrations in NaH_2PO_4 solution with an Al-Ti oxide dosage of 0.2 g/L in 100 mL of solution. The initial pH of the solutions was adjusted to 6.8 by adding H_2SO_4 or NaOH. After a few hours of continuous stirring, the suspensions were separated by centrifugation (2500 rpm, 20 min). P concentrations in the supernatant solutions were measured by the molybdenum blue method [32] using an ultraviolet-visible spectrophotometer (721N, Shanghai Spectrum, Shanghai, China) at a wavelength of 700 nm. To evaluate the temperature involved in P removal, similar experiments, as described above, were performed by transferring the sealed reaction vessel to a thermostatic shaker bath (293 K, 303 K, 313 K, and 323 K). The P solutions with P concentration ranging from 2.5 to 50 mg/L were prepared from a stock solution. The P removal efficiency (R) was calculated by Equation (1):

$$R = \frac{(C_0 - C_e)}{C_0} \times 100 \quad (1)$$

and the adsorption capacity of P at equilibrium (q_e) and at time t (q_t) were calculated by Equations (2) and (3):

$$q_e = \frac{V(C_0 - C_e)}{W} \quad (2)$$

$$q_t = \frac{V(C_0 - C_t)}{W} \quad (3)$$

where R denotes the removal efficiency (%), q_e and q_t denote the amount of phosphorus adsorbed at equilibrium and time t , respectively ((mg-P)/g), and C_0 and C_e are the initial and equilibrium concentrations of P in aqueous solution (mg/L), respectively. C_t is the P concentration at time t (mg/L). V denotes the volume of P solution (L), and W is the adsorbent weight (g). Each experiment was conducted three times and the average values were used for calculation.

After performing P adsorption, the used adsorbent was collected and washed thoroughly with water. The spent Al-Ti oxide adsorbent was immersed in 0.1 M NaOH solution for 4 h for regeneration. The material was filtered, repeatedly washed with water, and subsequently dried at room temperature under vacuum. The reusability of the regenerated sample was evaluated through adsorption of 15.0 mg/L P solution.

3. Results and Discussion

3.1. Optimization of Al-Ti Oxide for Adsorption of Phosphate

Al-Ti bimetal oxide with different Al:Ti molar ratios (1:0, 4:1, 2:1, 1:1, 1:2, 1:4, 0:1) were synthesized and their P removal capacities are compared in Figure 1. The comparison shows that sorption capacity was 50.7 mg/g on aluminum oxide (Al(III):Ti(IV) = 1:0) and 24.7 mg/g on titanium oxide (Al(III):Ti(IV) = 0:1). The adsorption capacities of Al-Ti bimetal oxide first increased and then decreased with an increase in Al-Ti molar ratio. The highest adsorption capacity was achieved at an Al-Ti molar ratio of 2:1, indicating that an appropriate amount of Al- and Ti-doping of the oxide hybrid enhanced the P adsorption capacity compared with individual oxides. The adsorption capacity of P on Al-Ti oxide was higher than that of Fe-Ti bimetal oxide, 32.95 mg/g (pH 6.8) [31]. It was also slightly higher than that of Fe-Al hydroxide, 51.8 mg/g (pH 4.5) [33], and that of Mg/Al layered double hydroxides, 54.9 mg/g (pH 6.0) [34]. A small amount of Ti doping into bimetal oxide obviously enhanced the P sorption capacity, while excessive Ti doping was detrimental to its sorption capacity. The results are similar to those reported in the literature [31]. The Ti^{4+} ions can make the surface charges more positive while attracting more phosphate ions. However, when the Ti content continues to increase, the P adsorption capacity of the adsorbent decreases. It is speculated that the effect of Ti content on P adsorption may be the result of the interaction of surface charge and surface microstructure. Therefore, the sorbent with an Al-Ti molar ratio of 2:1 was selected and applied in subsequent characterization and adsorption experiments.

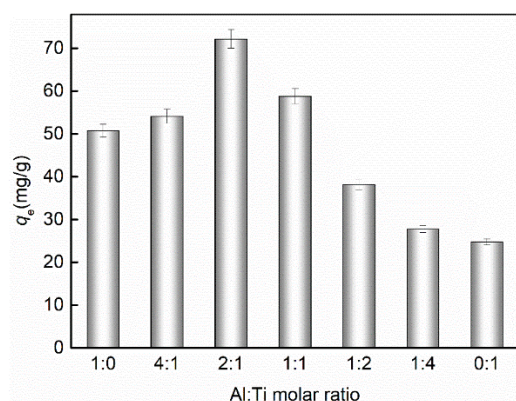


Figure 1. Comparison of phosphorus adsorption using sorbents with different Al and Ti molar ratios, initial pH of 6.8, initial P concentration = 50 mg/L, adsorbent dosage = 0.2 g/L, T = 298 K.

3.2. Characterization of Al-Ti Oxide

SEM photographs of the sorbent with an Al-Ti molar ratio of 2:1, together with Al-oxide (1:0) and Ti-oxide (0:1), are shown in Figure 2a–f. Two magnifications of 1000 \times and 5000 \times are given for each sample. The Al-oxide (a, b) has a rough surface and porous structure. Ti-oxide (c, d) is more likely to agglomerate. The Al-Ti sorbents (e, f) were

aggregates of many tiny nanoparticles and formed a rough surface. The dimensions of these nanoparticles were in the range of several tens of nanometers. EDS analysis (Figure 2g) revealed that the molar ratio of Al:Ti was approximately 13:10, which is slightly lower than that in the preparation process (2:1). Furthermore, there were peaks for elemental S on the surface of the sorbent, which is related to residual $\text{Al}_2(\text{SO}_4)_3$ and $\text{Ti}(\text{SO}_4)_2$ used in the preparation of Al-Ti oxide.

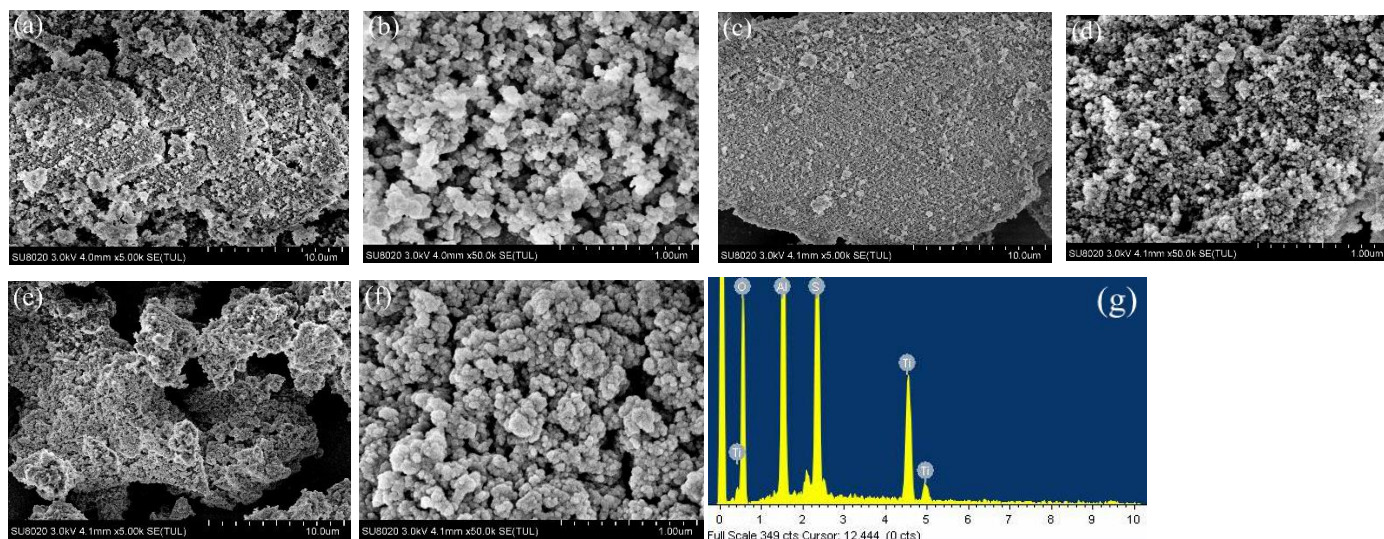


Figure 2. SEM photograph of Al-Ti oxide sorbent: (a) 5000 \times , (b) 50,000 \times ; Al-oxide (c) 5000 \times , (d) 50,000 \times ; and Ti-oxide (e) 5000 \times , (f) 50,000 \times ; (g) EDS of photograph of Al-Ti oxide.

The XRD pattern of the sorbent with an Al-Ti molar ratio of 2:1 is shown in Figure 3. The presence of Al_2O_3 in the adsorbent corresponds to the diffraction peaks of $2\theta = 25.6^\circ$, 43.4° , and 57.5° for the (012), (113), and (116) crystal planes, respectively (JCPDS card no. 76-1782). The diffraction peaks at 20.6° , 22.0° , 22.7° , 27.0° , 39.5° , 41.9° , 47.6° , and 76.2° can be assigned to the (200), (110), (111), (211), (312), (114), (313), and (135) crystal planes of $\text{Al}(\text{OH})_3$, respectively (JCPDS card no. 75-1863). The peaks at approximately 31.6° , 33.3° , and 36.0° were confirmed as the (026), (022), and (124) crystal planes of Ti_6O_{11} , respectively (JCPDS card no. 18-1401). These data indicate that Al-Ti oxide was successfully combined to form a hybrid material through the co-precipitation method.

The FT-IR spectra of the composite adsorbent in its original state, after P adsorption and after subsequent regeneration using 0.1 M NaOH solution, are illustrated in Figure 4. For the Al-Ti oxide hybrid material, the broad peak displayed at $3600\text{--}3200\text{ cm}^{-1}$ can be assigned to the O-H stretching mode of the hydrogen-bond, which implies the presence of water molecules [35]. The peak at approximately 1440 cm^{-1} corresponds to O-H deformation vibration [36]. The band at 1073 cm^{-1} can be attributed to Al-OH bending vibration [37]. The band from $500\text{ to }700\text{ cm}^{-1}$ could be due to metal-oxygen-metal vibrations [38]. The band at 1092 cm^{-1} and 696 cm^{-1} can be attributed to the asymmetric stretch vibration and bending vibration of S-O in the residual sulfate radical.

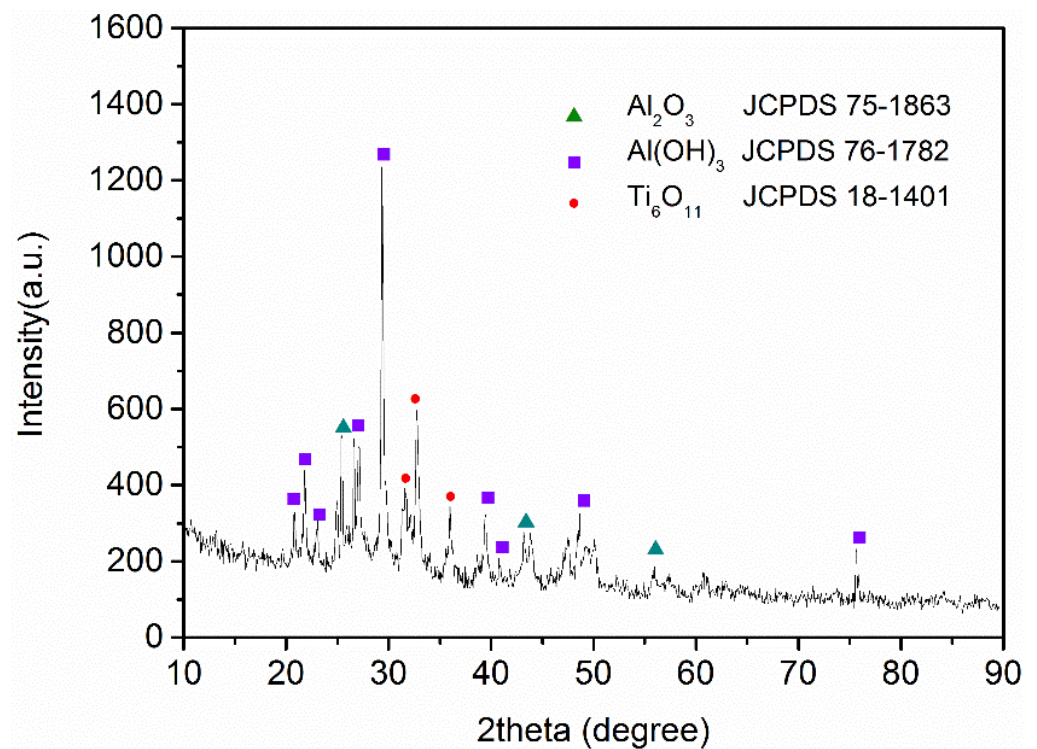


Figure 3. XRD pattern of the synthesized Al-Ti sorbent, Al-Ti molar ratio of 2:1.

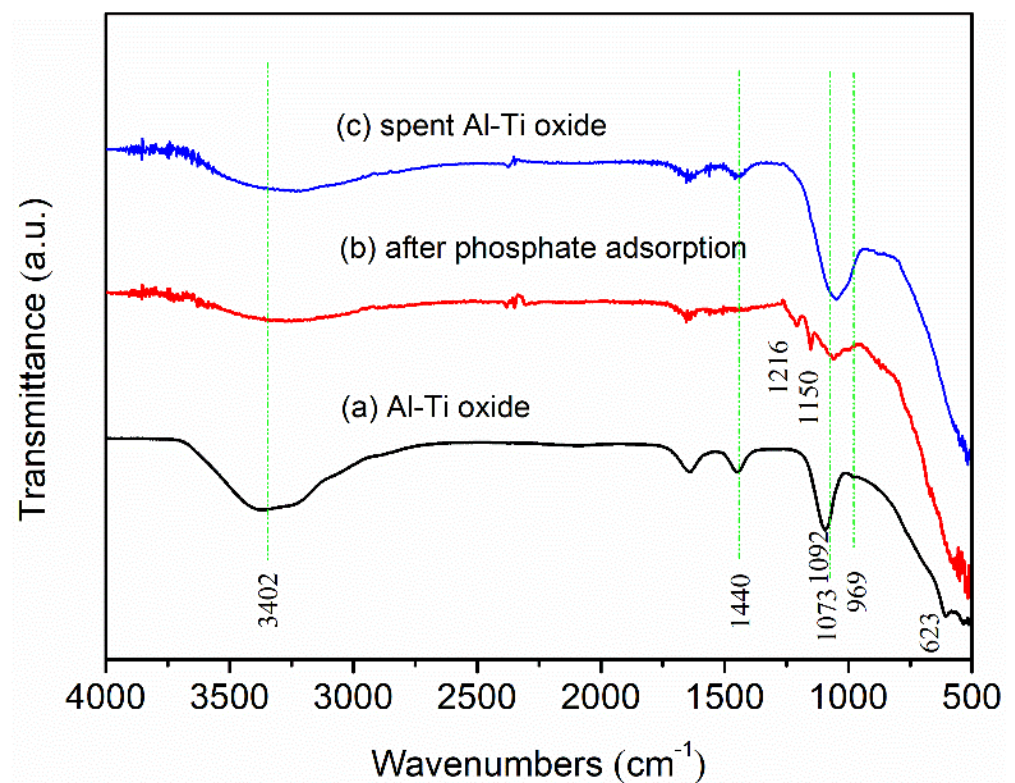


Figure 4. FT-IR spectra of sorbent (a) as-prepared (b) after adsorption of phosphate, and (c) spent Al-Ti oxide.

After Al-Ti oxide was immersed with the P solution, some new bands are observed at 1216 cm^{-1} and 1150 cm^{-1} . The band at 1216 cm^{-1} is assigned to the P stretching mode. The weaker band at 1150 cm^{-1} is ascribed to the stretching vibration of PO_2 [39]. The results

confirm that a surface complex (M-O-P) between P and Al-Ti oxide may be formed and that the P is adsorbed onto the surface of Al-Ti oxide successfully.

The Al-Ti oxide used after P adsorption was regenerated with 0.1 M NaOH solution. For the regenerated sample, the characteristic bands for O-H groups and the Al-OH group were recovered; the peaks for P groups at 1216 cm^{-1} and 1150 cm^{-1} were greatly weakened. Little to no change in the many peaks of the regenerated sample was observed compared with the as-prepared Al-Ti oxide. This indicates that the adsorption performance of P onto Al-Ti oxide could be recovered by regeneration with the NaOH solution. The zeta potential curve of Al-Ti oxide was presented in Figure 5, which indicates that the point of zero charge (PZC) is about zero at pH 8, and that the charge is in the range from 24 to -28 mV at pH 3–11. Therefore, this should be a stable adsorbent toward cationic adsorbate because of its slight basic pH_{PZC} and relatively large positive potential in neutral solution.

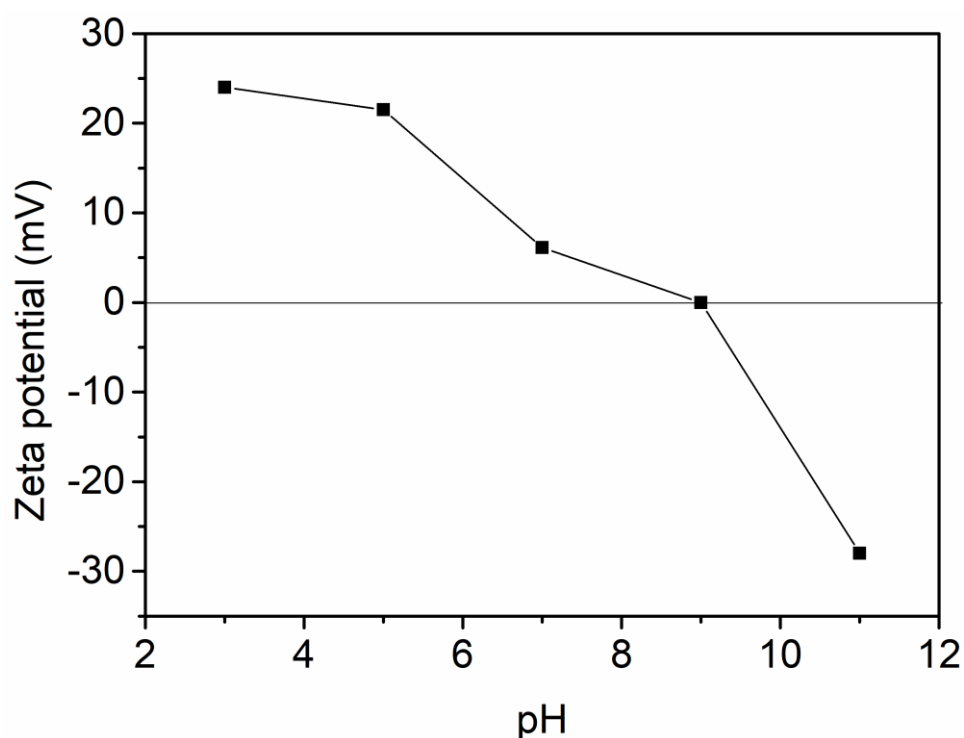


Figure 5. Effect of initial pH on zeta potential of Al-Ti oxide.

The N_2 adsorption-desorption isotherms of Al-Ti bimetal oxide are shown in Figure 6a. According to IUPAC classification, the adsorption-desorption isotherms follow type IV isotherms, indicating the existence of a mesoporous structure in Al-Ti bi-metal oxide [40]. This oxide also exhibits an H_3 -type hysteresis loop in the range of relatively high P/P_0 , which can be attributed to slit-shaped pores [31]. The formation of this kind of pore structure is attributed to the uneven aggregation of tiny nanoparticles. Surface area measurements of Al-Ti oxides are summarized in Table 1. The Al-Ti oxide has a surface area of $3.94\text{ m}^2/\text{g}$ and an average pore size of 12.1 nm . The pore size distribution of the synthesized Al-Ti oxide is shown in Figure 6b. The pores are mainly mesopores, ranging from 2 to 50 nm in size.

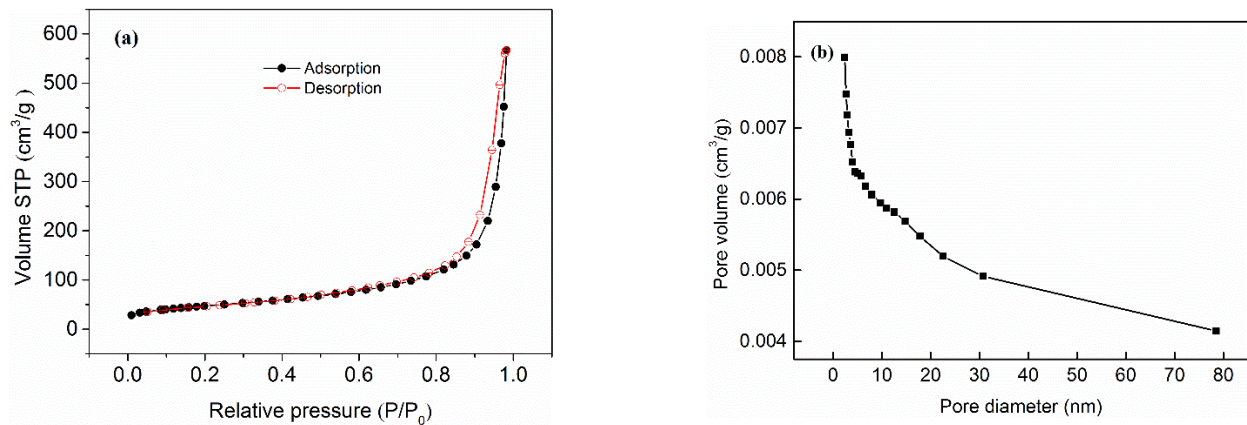


Figure 6. (a) N₂ adsorption-desorption isotherm and (b) pore size distribution curve of Al-Ti oxide.

Table 1. Surface area measurements of Al-Ti oxide, Al oxide, and Ti oxide.

	BET Surface Area (m ² /g)	Micropore Area (m ² /g)	Average Pore Diameter (nm)
Al-Ti oxide	3.94	1.79	12.1
Al oxide	5.52	3.43	20.2
Ti oxide	2.36	1.26	10.6

3.3. Adsorption Kinetics

Figure 7a displays the effect of contact time on P adsorption onto Al-Ti oxide. The adsorbed amount of P increased with an increase in contact time. The adsorption equilibrium for P was achieved after about 12 h. The rapid adsorption observed during the initial stage was probably due to the abundant availability of adsorption sites on the Al-Ti oxide surface; then, the adsorption became less efficient with gradual occupancy of the adsorption sites.

To predict the adsorption kinetics of P onto Al-Ti oxide, two adsorption kinetic models, including pseudo-first-order and pseudo-second-order models were applied to examine the adsorption process [41–43]. The pseudo-first-order and pseudo-second-order models can be represented by Equations (4) and (6), and their linear forms as Equations (5) and (7) when integrating the two equations for the boundary conditions of $q_t = 0$ at $t = 0$ and $q_t = q_t$ at $t = t$, respectively:

$$\frac{dq_t}{dt} = k_1(q_e - q_t) \quad (4)$$

$$\frac{dq_t}{dt} = k_2(q_e - q_t)^2 \quad (5)$$

$$q_t = q_e(1 - e^{-k_1 t}) \quad (6)$$

$$\frac{t}{q_t} = \frac{1}{k_2 q_e^2} + \frac{1}{q_e} t \quad (7)$$

where q_e (mg/g) and q_t (mg/g) are the amount of P adsorbed onto Al-Ti oxide at equilibrium and at time t (min), respectively. k_1 (1/min) and k_2 (g/mg min) are the rate constants of the pseudo-first-order and pseudo-second-order models, respectively.

The fitting of the two kinetic models for P adsorption with various initial concentrations are shown in Figure 7b–c. Kinetic parameters fit by the pseudo-first-order and pseudo-second-order models were calculated and are listed in Table 2. The coefficients of determination (r^2) of the pseudo-second-order model were higher than those of pseudo-second-order mode, and the calculated q_e values were in good agreement with experimental results, verifying that the adsorption process could be better described by the pseudo-second-order model.

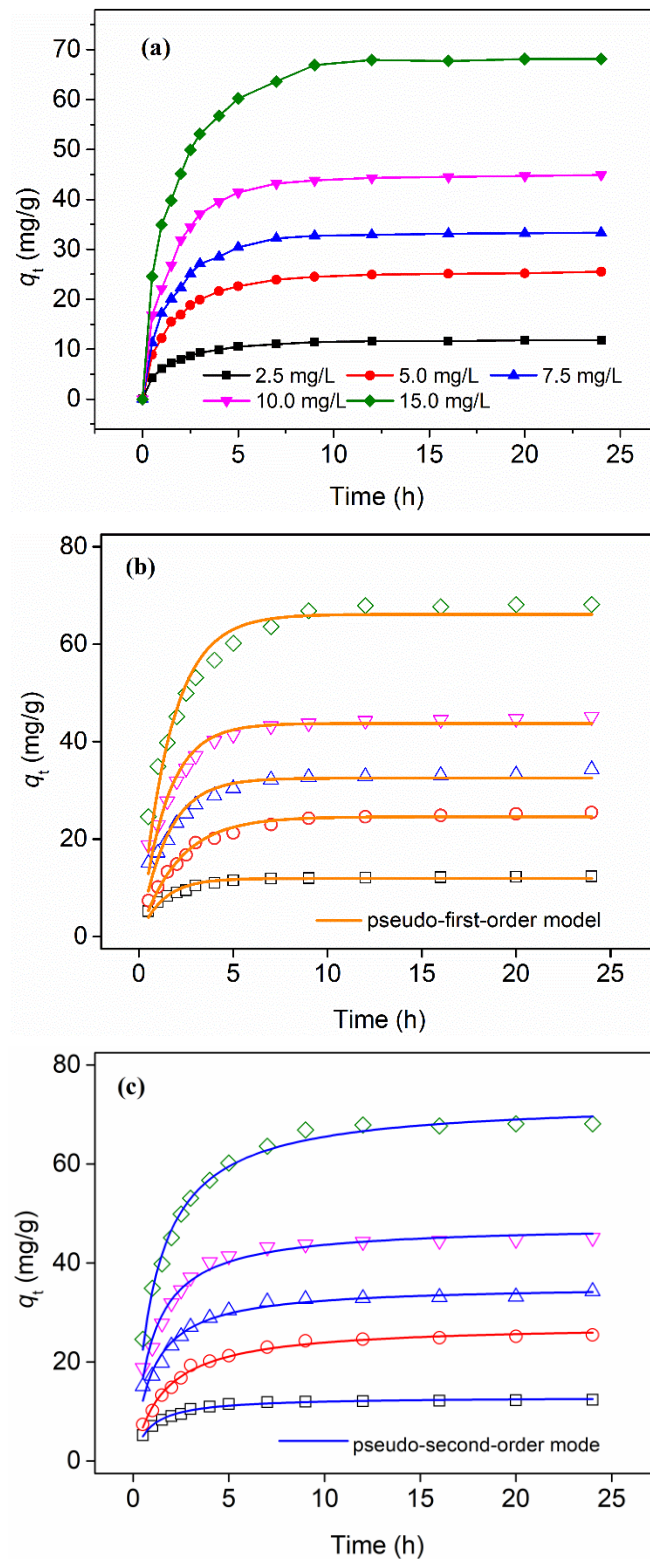


Figure 7. (a) Effect of contact time and initial concentration on P adsorption on Al-Ti oxide adsorbent; (b) adsorption kinetics fit by pseudo-first-order (dashed lines) and (c) pseudo-second-order (solid lines) models with P initial concentration of 2.5, 5.0, 7.5, 10.0, and 15.0 mg/L, adsorbent dosage = 0.2 g/L, T = 298 K.

Table 2. Adsorption kinetic parameters of P onto Al-Ti oxide adsorbent fit by pseudo-first-order and pseudo-second-order models.

Initial P Concentration, mg/L	Pseudo-First-Order Model			Pseudo-Second-Order Model		
	k_1 (1/h)	q_e (mg/g)	R^2	k_2 g/(mg·h)	q_e (mg/g)	R^2
2.5	0.801	11.9	0.941	0.0971	13.0	0.990
5.0	0.488	24.6	0.977	0.0236	27.6	0.991
7.5	0.679	32.5	0.907	0.0294	35.5	0.968
10.0	0.701	43.7	0.949	0.0225	47.7	0.980
15.0	0.612	66.1	0.948	0.0123	72.8	0.991

3.4. Adsorption Isotherms

Adsorption isotherms are significant for describing the interaction between adsorbate and adsorbent, and for optimizing the employment of adsorbents. Thus, the analysis of equilibrium isotherms is fundamental for evaluating the adsorption mechanism. P adsorption isotherms at 293 K, 303 K, 313 K, and 323 K obtained by varying equilibrium concentration (C_e) are illustrated in Figure 8a. The initial P concentrations were 2.5, 5.0, 7.5, 10.0, 15.0, and 50.0 mg/L, and the P adsorption capacities increased with an increase in initial concentration. Higher adsorption capacity was also achieved at higher temperatures, which reveals the greater mobility of P in solution and higher probability of collision between adsorption sites and PO_4^{3-} ions [44]. The fitting of experimental data to six different isotherm models is shown in Figure 8b–g; the estimated parameters for each model are summarized in Table 3.

3.4.1. Langmuir Isotherm

The Langmuir isotherm [45,46] is based on the adsorption process, which is uniform and monolayer on the surface of the adsorbent. It is calculated as Equation (8):

$$\frac{C_e}{q_e} = \frac{1}{bQ_m} + \frac{C_e}{Q_m} \quad (8)$$

where q_e is the number of P ions adsorbed at equilibrium (mg/g), Q_m is the maximum monolayer adsorption capacity (mg/g), and b is the Langmuir isotherm constant related to adsorption energy (L/mg) [47]. Figure 8b shows Langmuir plots for P removal at different temperatures.

The feasibility of the adsorption process was determined on the basis of the equilibrium parameter/dimensionless constant separation factor R_L expressed by Equation (9):

$$R_L = \frac{1}{1 + bC_0} \quad (9)$$

where C_0 is the initial P concentration (mg/L). The values of R_L indicate whether the type of adsorption is unfavorable ($R_L > 1$), linear ($R_L = 1$), favorable ($0 < R_L < 1$), or irreversible ($R_L = 0$) [48]. The constants and R_L values are listed in Table 2.

The r^2 values ranged from 0.897 to 0.998, which means that the adsorption data had good fit with the Langmuir model. This result shows monolayer adsorption on a homogenous surface in nature, and the maximum adsorption capacity of phosphorus ions on the sorbent is 70.7 mg/L at 323 K. The R_L values are between 0 and 1, demonstrating the material's high selectivity toward PO_4^{3-} , and the adsorption is favorable.

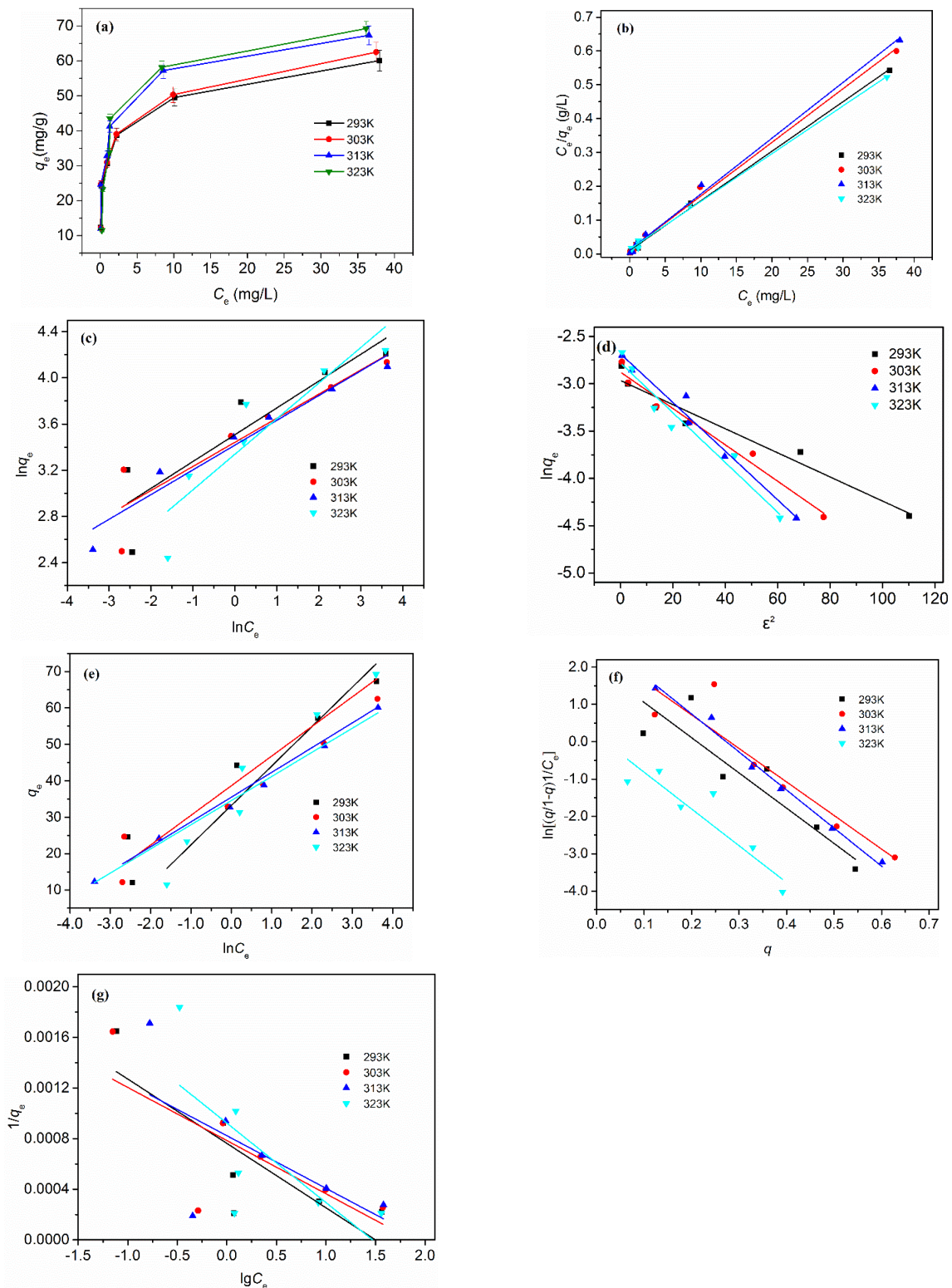


Figure 8. Adsorption isotherm of phosphorus on Al-Ti oxide composite sorbent: (a) adsorptive experiments with various equilibrium concentrations of P, (b) Langmuir, (c) Freundlich, (d) D-R, (e) Temkin, (f) Frumkin, and (g) Harkin–Jura model. The average value in (a) was used for calculations in (b–g), adsorbent dosage = 0.2 g/L, equilibrium time = 8 h, pH = 6.8.

Table 3. Adsorption isotherm data of various isotherm models.

Parameter	293 K	303 K	313 K	323 K
Langmuir				
Q_m (mg/g)	68.2	63.0	60.5	70.7
b (L/mg)	0.691	0.759	0.701	0.958
R_L	0.028	0.026	0.028	0.020
r^2	0.998	0.995	0.996	0.998
Freundlich				
K_F (L/g)	33.4	1.23	1.24	1.36
n	4.31	4.80	4.67	3.25
r^2	0.768	0.810	0.942	0.795
D-R				
Q_{DR} (mg/g)	51.3	56.2	68.2	61.9
$\beta \times 10^{-3}$ (mol ² /kJ ²)	12.7	19.2	25.7	26.3
E (kJ/mol)	6.28	5.10	4.41	4.36
r^2	0.955	0.977	0.975	0.952
Temkin				
K_T (L/mg)	4.75	5.22	5.21	1.88
B (kJ/mol)	7.93	6.80	6.63	10.83
r^2	0.919	0.931	0.993	0.944
Frumkin				
a	−4.72	−4.49	−5.10	−4.93
$\ln k$	2.00	2.52	2.78	0.169
ΔG (kJ/mol)	4.87	6.34	7.24	0.455
r^2	0.834	0.869	0.988	0.836
Harkin–Jura				
$A \times 10^3$	1.97	2.38	2.41	1.59
B	1.50	1.87	1.98	1.47
r^2	0.603	0.457	0.263	0.384

3.4.2. Freundlich Isotherm

The Freundlich isotherm [49], utilized for heterogeneous systems with non-equivalent binding sites, is given by Equation (10):

$$\ln q_e = \ln K_F + \frac{1}{n} \ln C_e \tag{10}$$

where K_F (L/g) and n are the Freundlich constants that indicate the capacity and intensity of the adsorption process, respectively [47]. Figure 8c gives the fitting curves for the Freundlich isotherm.

From Table 1, comparison of correlation coefficients of Langmuir and Freundlich isotherms shows that the Freundlich model is not appropriate for describing the adsorption process. The values of n ranged between 1 and 10, which indicates favorable sorption of P.

3.4.3. Dubinin–Radushkevick (D-R) Isotherm

The D-R isotherm [50,51] was employed to model was used to study the mean adsorption energy, and is described by Equation (11):

$$\ln q_e = \ln Q_{DR} - \beta_{DR} \varepsilon^2 \tag{11}$$

where Q_{DR} is the monolayer saturation capacity (mg/g), and β_{DR} is the D-R adsorption energy constant related to mean adsorption energy (mol²/J²). ε is the Polanyi potential expressed as Equation (12):

$$\varepsilon = RT \ln \left[\frac{C_0}{C_e} \right] \tag{12}$$

where R is the gas constant (kJ/mol K), and T is the temperature (K). The mean adsorption energy E (kJ/mol) can be calculated by Equation (13):

$$E = \frac{1}{\sqrt{2\beta}} \quad (13)$$

A value of E under 8 kJ/mol is for physical adsorption and ranges from 8.0 to 16.0 kJ/mol for chemical processes [37]. Fitting of the experimental results to the D-R isotherm is shown in Figure 8d.

The value of the mean free energy (E) of adsorption is 4.36–6.28 kJ/mol, which reveals that the type of P adsorption onto Al-Ti oxide follows a physical adsorption mechanism.

3.4.4. Temkin Isotherm

The Temkin model [52] assumes that the free energy of adsorption is a function of the surface coverage due to adsorbent-adsorbate interactions, and is expressed as Equation (14):

$$q_e = B \ln K_T C_e \quad (14)$$

where B is involved with the heat of adsorption. K_T is the Temkin isotherm equilibrium binding constant (L/mg), calculated as Equation (15):

$$B = \frac{RT}{b_T} \quad (15)$$

where b_T is the Temkin isotherm constant [53]. The plots of q_e versus $\ln C_e$ are given in Figure 8e. The Temkin isotherm shows good agreement with $r^2 > 0.90$. In Table 1, K_T increases with increasing temperature (293–313 K) and then decreases at 323 K, indicating stronger interaction between P and sorbent with an increase in temperature (293–313 K), followed by reduced interaction. It can be observed from B that the heat of adsorption is maximum at 313 K and minimum at 323 K.

The B values obtained from the Temkin isotherm were: 7.93 kJ/mol, 6.80 kJ/mol and 6.63 kJ/mol at the temperature of 293 K, 303 K, 313 K, respectively, which indicates that adsorption of P on Al-Ti oxide composite sorbent takes place by physisorption. The binding energy value was < 8 kJ/mol, thus physical adsorption is the mechanism involved. In the physical adsorption process, adsorbates adhere to the adsorbent through weak van der Waals interactions, and, thus, this process is associated with relatively low adsorption energies. The B value at 323 K was > 8 kJ/mol, suggesting that the chemisorption occurs at relatively high temperatures [54].

3.4.5. Frumkin Isotherm

The Frumkin model [55] accounts for interaction between adsorbed species. It is presented as Equation (16):

$$\ln \left[\left(\frac{\theta}{1-\theta} \right) \frac{1}{C_e} \right] = \ln k + 2a\theta \quad (16)$$

where θ is the fractional occupation ($\theta = q_e/q_m$); q_m is the theoretical monolayer saturation capacity (mg/g) determined by D-R isotherm; and a is the interaction coefficient, the value of which is positive for attraction and negative for repulsion. When a is zero, there is no interaction between the adsorbate species [53]. Fitting curves of θ versus $\ln \left[\left(\frac{\theta}{1-\theta} \right) \frac{1}{C_e} \right]$ are shown in Figure 8. k is relevant to the adsorption equilibrium and written as Equation (17):

$$\ln k = \frac{-\Delta G}{RT} \quad (17)$$

where ΔG is the Gibbs free energy (J/mol). The Frumkin isotherm constants are listed in Table 2. Fitting of the experimental results with the Frumkin isotherm is shown in Figure 8f.

It can be noted from Table 1 that the negative a values suggest that repulsion exists between the adsorbed species. The negative values of ΔG demonstrate that the adsorption process is spontaneous in nature.

3.4.6. Harkin–Jura Isotherm

The Harkin–Jura isotherm [56] takes into account multilayer adsorption and can be interpreted by the existence of a heterogeneous pore distribution. It can be represented as Equation (18):

$$\frac{1}{q_e^2} = \left(\frac{B}{A}\right) - \left(\frac{1}{A}\right) \lg C_e \quad (18)$$

where A and B are the Harkin–Jura isotherm parameters [53]. Fitting curves for the Harkin–Jura isotherm are illustrated in Figure 8g.

It is observed that the Harkin–Jura isotherm has a relatively low r^2 value. It follows multilayer adsorption, in accordance with the conclusion made with the Langmuir isotherm that the adsorption process is uniform and monolayer.

It is clear from Table 3 that Langmuir, D-R, and Temkin models represent the sorption results well. The description of P adsorption onto Al-Ti oxide points to the following: (i) P adsorption occurs on the homogeneous surface of Al-Ti oxide; the number of identical adsorption sites is finite. R_L values ranging from 0 to 1 indicate the favorable nature of adsorption. (ii) The value of the mean free energy (E) of adsorption is 4.41–6.28 kJ/mol from the D-R model, suggesting that the type of P adsorption on the sorbent can be defined as physiochemical adsorption. (iii) The Temkin isotherm suggests that the maximum value of K_T and minimum value of B are 5.21 L/mg and 6.63 kJ/mol at 313 K, respectively, which explains the equilibrium binding energy and maximum heat of adsorption at 313 K. The higher temperature of 323 K shows irregular adsorption energy; it can be inferred that the adsorption mechanism had changed at high temperature.

The monolayer adsorption capacity of P on the similar sorbents were listed in Table 4. Compared with the reported sorbents, the Al-Ti bimetal oxide composite exhibited a competitive capacity.

Table 4. Comparison of phosphate adsorption capacity among different adsorbents.

Adsorbent	pH	Temp (K)	Dose (g/L)	q_m (mg/g)	References
Fe-Ti bimetal oxide	4.5	293	0.2	32.95	[31]
Fe-Al hydroxide	6.0	298	1.0	51.80	[33]
Mg/Al LDHS	6.0	298	0.6	54.90	[34]
Amorphous ZrO ₂	6.2	298	0.1	99.00	[57]
Modified La ₂ O ₃	5.6	298	0.5	58.70	[58]
Al-Ti bimetal oxide	6.8	293	0.2	68.20	This study

3.5. Thermodynamic Studies

Different thermodynamic parameters Gibbs free energy change (ΔG), enthalpy change (ΔH), and entropy change (ΔS) for the adsorption of P onto Al-Ti bimetal oxide composite were calculated using the following equations:

$$\Delta G = -RT \ln K_c \quad (19)$$

where R is the gas constant (8.314 J/mol K). K_C is the equilibrium constant and defined in Equation (20):

$$K_C = \frac{C_A}{C_S} \quad (20)$$

where C_A and C_S are the equilibrium concentrations of P on Al-Ti oxide adsorbent (mg/L) and in solution (mg/L), respectively [41]. Standard enthalpy (ΔH) and entropy (ΔS) of adsorption can be estimated from van't Hoff equation (Equation (21)):

$$\ln K_C = \frac{-\Delta H}{RT} + \frac{\Delta S}{R} \quad (21)$$

The plot of $\ln K_C$ versus $\frac{1}{T}$ is given in Figure 9.

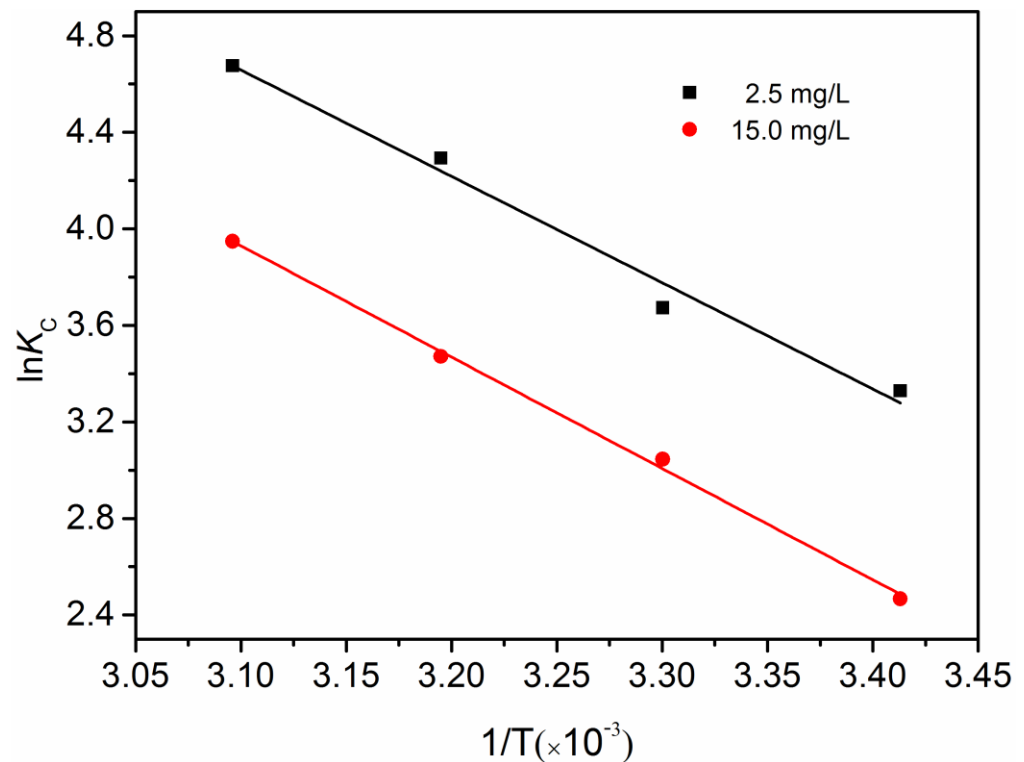


Figure 9. Plot of $\ln K_C$ versus $1/T$ for phosphorus sorption onto Al-Ti bimetal oxide.

Thermodynamic parameters estimated for P adsorption in the temperature range of 293 K–313 K are shown in Table 5.

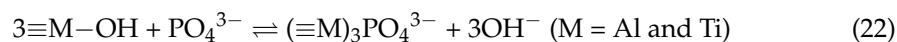
Table 5. Thermodynamic parameters of P adsorption on Al-Ti oxide.

Concentration (mg/L)	$-\Delta G$ (kJ/mol)			ΔH (kJ/mol)	ΔS (J/mol K)
	293 K	303 K	313 K		
2.5	8.11	9.25	11.17	36.62	152.25
15.0	6.01	7.67	9.03	38.36	151.58

From Table 4, the positive value of ΔH confirms that P adsorption on Al-Ti oxide is an endothermic reaction due to increased adsorption from successive increases in temperature [59]. The value of ΔG is more negative with increased temperature, showing that spontaneous reaction is enhanced by temperature. The ΔG values varied in range from 6.01 to -11.17 kJ/mol, revealing that physisorption contributes to the adsorption mechanism (physical range for ΔG^0 is $-20 < \Delta G^0 < 0$ kJ/mol and chemical range is $-80 < \Delta G^0 < -400$ kJ/mol) [60,61]. The value of enthalpy (ΔH) shows physical adsorption (less than 40 kJ/mol for physisorption and 80–450 kJ/mol for chemisorption) [62,63]. The positive ΔS value elaborates increased randomness at the solid/solution interface during P adsorption on Al-Ti hydroxide.

3.6. Regeneration of Spent Sorbent

According to the literature, P sorption on bimetal oxide occurs via the replacement of surface hydroxyl groups (M-OH) by P to form inner-sphere complexes [31]. The metal oxide was effectively regenerated by NaOH solution. The P adsorption process can be described as:



As P adsorption onto Al-Ti oxide proceeds over time, the adsorption active sites of the sorbent gradually became saturated with P, causing a reduction in adsorption capacity. It can be anticipated that improved adsorption occurs through sorbent regeneration. The results of consecutive adsorption/regeneration cycles are illustrated in Figure 10. Compared with the adsorption capacity of 68.9 mg P/g and removal rate of 93.6% in the first use of Al-Ti oxide, the adsorption capacity and P removal rate reached 57.6 mg/g and 76.9%, respectively, after five consecutive adsorption/regeneration cycles. Therefore, it can be concluded that Al-Ti oxide exhibited good reusability for P removal.

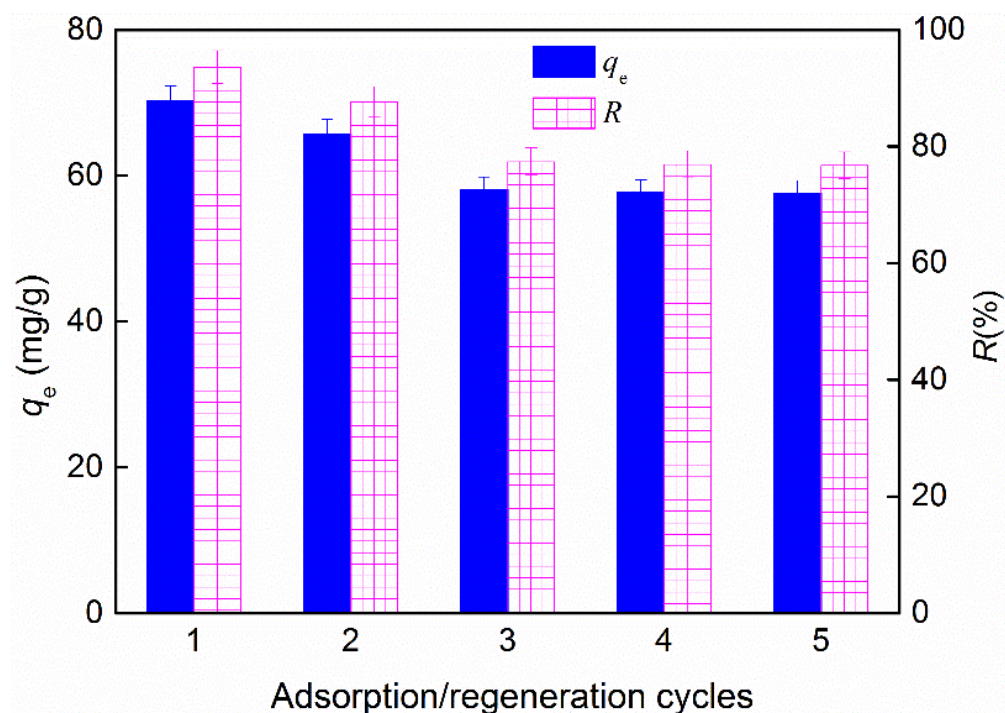


Figure 10. Results of phosphate adsorption/regeneration cycles.

4. Conclusions

In this research, adsorption of phosphate from aqueous solution was investigated using a novel Al-Ti oxide composite sorbent. The Al-Ti bimetal oxide prepared with an Al/Ti molar ratio of 2:1 showed high P sorption capacity. Kinetic analysis showed that the adsorption process of the P onto Al-Ti oxide composite was more consistent with the second-order-kinetic models. Langmuir, D-R, and Temkin isotherms could better describe the experimental data. Langmuir monolayer sorption capacity for P was 68.2 mg/g at pH 6.8, which outperforms most reported bimetal oxide-based sorbents. The spent Al-Ti oxide sorbent could be successfully regenerated by 0.1 M NaOH solution. Thermodynamic experiments showed that P adsorption onto Al-Ti sorbent is a feasible, spontaneous, and endothermic sorption process. Future work needs to supplement more advanced characterization methods to explore the adsorption mechanism.

Author Contributions: Conceptualization, X.W. (Xuefeng Wei) and J.M.; software, R.Z.; validation, Z.L., X.W. (Xiaoyang Wan) and N.Z.; formal analysis, R.Z.; investigation, X.W. (Xiaoyang Wan); resources, X.W. (Xuefeng Wei); data curation, X.W. (Xiaoyang Wan); writing—original draft preparation, X.W. (Xiaoyang Wan); writing—review and editing, X.W. (Xuefeng Wei); visualization, R.Z.; supervision, X.W. (Xuefeng Wei); project administration, X.W. (Xuefeng Wei); funding acquisition, S.P. All authors have read and agreed to the published version of the manuscript.

Funding: This research was funded by [National Natural Science Foundation of China] grant number [21403058 and 22175057], and Key Scientific Research Projects of Higher Education Institutions in Henan Province, China [20A610001]. And the APC was funded by [22175075].

Institutional Review Board Statement: Not applicable.

Informed Consent Statement: Not applicable.

Data Availability Statement: Not applicable.

Acknowledgments: I acknowledge the support of Henan University of Science and Technology.

Conflicts of Interest: The authors declared that they have no conflict of interest.

References

1. Nguyen, T.A.H.; Ngo, H.H.; Guo, W.S.; Zhang, J.; Liang, S.; Lee, D.J.; Nguyen, P.D.; Bui, X.T. Modification of agricultural waste/by-products for enhanced phosphate removal and recovery: Potential and obstacles. *Bioresour. Technol.* **2014**, *169*, 750–762. [[CrossRef](#)] [[PubMed](#)]
2. Zhang, L.; Jin, S.; Wang, Y.; Ji, J. Phosphate adsorption from aqueous solution by lanthanum-iron hydroxide loaded with expanded graphite. *Environ. Technol.* **2018**, *39*, 997–1006. [[CrossRef](#)] [[PubMed](#)]
3. Wang, D.; Chen, N.; Yu, Y.; Hu, W.; Feng, C. Investigation on the adsorption of phosphorus by Fe-loaded ceramic adsorbent. *J. Colloid Interface Sci.* **2016**, *464*, 277–284. [[CrossRef](#)] [[PubMed](#)]
4. Hakanson, L.; Bryhn, A.C.; Hytteborn, J.K. On the issue of limiting nutrient and predictions of cyanobacteria in aquatic systems. *Sci. Total Environ.* **2007**, *379*, 89–108. [[CrossRef](#)]
5. Smith, V.H. Eutrophication of freshwater and coastal marine ecosystems a global problem. *Environ. Sci. Pollut. Res.* **2003**, *10*, 126–139. [[CrossRef](#)]
6. Begum, S.A.; Hyder, A.; Hicklen, Q.; Crocker, T.; Oni, B. Adsorption characteristics of ammonium onto biochar from an aqueous solution. *J. Water Supply Res. Technol. AQUA* **2020**, *70*, 113–122. [[CrossRef](#)]
7. Johnson, P.T.J.; Chase, J.M.; Dosch, K.L.; Hartson, R.B.; Gross, J.A.; Larson, D.J.; Sutherland, D.R.; Carpenter, S.R. Aquatic eutrophication promotes pathogenic infection in amphibians. *Proc. Natl. Acad. Sci. USA* **2007**, *104*, 15781–15786. [[CrossRef](#)]
8. Schindler, D.W.; Hecky, R.E.; Findlay, D.L.; Stainton, M.P.; Parker, B.R.; Paterson, M.J.; Beaty, K.G.; Lyng, M.; Kasian, S.E.M. Eutrophication of lakes cannot be controlled by reducing nitrogen input: Results of a 37-year whole-ecosystem experiment. *Proc. Natl. Acad. Sci. USA* **2008**, *105*, 11254–11258. [[CrossRef](#)]
9. Schindler, D.W.; Carpenter, S.R.; Chapra, S.C.; Hecky, R.E.; Orihel, D.M. Reducing phosphorus to curb lake eutrophication is a success. *Environ. Sci. Technol.* **2016**, *50*, 8923–8929. [[CrossRef](#)]
10. Chen, X.; Cheng, X.; Sun, D.; Ma, W.; Wang, X. Adsorptive removal of phosphate from secondary effluents in WWTPs by ZnAl layered double hydroxides granules. *Desalin. Water Treat.* **2015**, *54*, 1216–1225. [[CrossRef](#)]
11. Huang, H.; Liu, J.; Zhang, P.; Zhang, D.; Gao, F. Investigation on the simultaneous removal of fluoride, ammonia nitrogen and phosphate from semiconductor wastewater using chemical precipitation. *Chem. Eng. J.* **2017**, *307*, 696–706. [[CrossRef](#)]
12. Peng, L.; Dai, H.; Wu, Y.; Peng, Y.; Lu, X. A comprehensive review of phosphorus recovery from wastewater by crystallization processes. *Chemosphere* **2018**, *197*, 768–781. [[CrossRef](#)]
13. Lee, W.H.; Bishop, P.L. In situ microscale analyses of activated sludge flocs in the enhanced biological phosphate removal process by the use of microelectrodes and fluorescent in situ hybridization. *J. Environ. Eng.* **2010**, *136*, 561–567. [[CrossRef](#)]
14. Yin, Q.; Zhang, B.; Wang, R.; Zhao, Z. Biochar as an adsorbent for inorganic nitrogen and phosphorus removal from water: A review. *Environ. Sci. Pollut. Res.* **2017**, *24*, 26297–26309. [[CrossRef](#)] [[PubMed](#)]
15. Wen, Z.; Zhang, Y.; Dai, C. Removal of phosphate from aqueous solution using nanoscale zerovalent iron (nZVI). *Colloids Surf. A* **2014**, *457*, 433–440. [[CrossRef](#)]
16. Karaca, S.; Gürses, A.; Ejder, M.; Açıkyıldız, M. Kinetic modeling of liquid-phase adsorption of phosphate on dolomite. *J. Colloid Interface Sci.* **2004**, *277*, 257–263. [[CrossRef](#)] [[PubMed](#)]
17. Moharami, S.; Jalali, M. Use of modified clays for removal of phosphorus from aqueous solutions. *Environ. Monit. Assess.* **2015**, *187*. [[CrossRef](#)]
18. Biswas, B.K.; Inoue, K.; Ghimire, K.N.; Ohta, S.; Harada, H.; Ohto, K.; Kawakita, H. The adsorption of phosphate from an aquatic environment using metal-loaded orange waste. *J. Colloid Interface Sci.* **2007**, *312*, 214–223. [[CrossRef](#)]
19. Tran, D.N.H.; Kabiri, S.; Wang, L.S.; Losic, D. Engineered graphene-nanoparticle aerogel composites for efficient removal of phosphate from water. *J. Mater. Chem. A* **2015**, *3*, 6844–6852. [[CrossRef](#)]

20. Li, G.; Gao, S.; Zhang, G.; Zhang, X. Enhanced adsorption of phosphate from aqueous solution by nanostructured iron(III)–copper(II) binary oxides. *Chem. Eng. J.* **2014**, *235*, 124–131. [[CrossRef](#)]
21. Meng, W.N.; Xie, J.; Wu, D.Y.; Zhang, Z.J.; Kong, H.N. Study on phosphate removal and recovery by activated alumina. *Environ. Sci.* **2013**, *34*, 231–236. (In Chinese)
22. Vodyanitskii, Y.N. Iron hydroxides in soils: A review of publications. *Eurasian Soil Sci.* **2010**, *43*, 1244–1254. [[CrossRef](#)]
23. Huang, Y.; Yang, J.-K.; Keller, A.A. Removal of arsenic and phosphate from aqueous solution by metal (hydr)-oxide coated sand. *ACS Sustainable Chem. Eng.* **2014**, *2*, 1128–1138. [[CrossRef](#)]
24. Kropacheva, T.N.; Antonova, A.S.; Kornev, V.I. The influence of aminopolycarboxylates on the sorption of copper (II) cations by (Hydro)oxides of iron, Aluminum, and manganese. *Eurasian Soil Sci.* **2016**, *49*, 765–772. [[CrossRef](#)]
25. Antelo, J.; Avena, M.; Fiol, S.; Lopez, R.; Arce, F. Effects of pH and ionic strength on the adsorption of phosphate and arsenate at the goethite-water interface. *J. Colloid Interface Sci.* **2005**, *285*, 476–486. [[CrossRef](#)] [[PubMed](#)]
26. Tofik, A.S.; Taddesse, A.M.; Tesfahun, K.T.; Girma, G.G. Fe–Al binary oxide nanosorbent: Synthesis, characterization and phosphate sorption property. *J. Environ. Chem. Eng.* **2016**, *4*, 2458–2468. [[CrossRef](#)]
27. Lu, J.; Liu, H.; Zhao, X.; Jefferson, W.; Cheng, F.; Qu, J. Phosphate removal from water using freshly formed Fe–Mn binary oxide: Adsorption behaviors and mechanisms. *Colloids Surf. A* **2014**, *455*, 11–18. [[CrossRef](#)]
28. Wan, S.; Wang, S.; Li, Y.; Gao, B. Functionalizing biochar with Mg–Al and Mg–Fe layered double hydroxides for removal of phosphate from aqueous solutions. *J. Ind. Eng. Chem.* **2017**, *47*, 246–253. [[CrossRef](#)]
29. Kang, S.A.; Li, W.; Lee, H.E.; Phillips, B.L.; Lee, Y.J. Phosphate uptake by TiO₂: Batch studies and NMR spectroscopic evidence for multisite adsorption. *J. Colloid Interface Sci.* **2011**, *364*, 455–461. [[CrossRef](#)]
30. Park, H.S.; Kwak, S.H.; Mahardika, D.; Mameda, N.; Choo, K.H. Mixed metal oxide coated polymer beads for enhanced phosphorus removal from membrane bioreactor effluents. *Chem. Eng. J.* **2017**, *319*, 240–247. [[CrossRef](#)]
31. Lu, J.; Liu, D.; Hao, J.; Zhang, G.; Lu, B. Phosphate removal from aqueous solutions by a nano-structured Fe–Ti bimetal oxide sorbent. *Chem. Eng. Res. Des.* **2015**, *93*, 652–661. [[CrossRef](#)]
32. He, Z.; Honeycutt, C.W. A modified molybdenum blue method for orthophosphate determination suitable for investigating enzymatic hydrolysis of organic phosphates. *Commun. Soil Sci. Plant Anal.* **2005**, *36*, 1373–1383. [[CrossRef](#)]
33. Wang, X.-H.; Liu, F.-F.; Lu, L.; Yang, S.; Zhao, Y.; Su, L.-B.; Wang, S.-G. Individual and competitive adsorption of Cr(VI) and phosphate onto synthetic Fe–Al hydroxides. *Colloids Surf. A* **2013**, *423*, 42–49. [[CrossRef](#)]
34. Novillo, C.; Guaya, D.; Allen-Perkins Avendaño, A.; Armijos, C.; Cortina, J.L.; Cota, I. Evaluation of phosphate removal capacity of Mg/Al layered double hydroxides from aqueous solutions. *Fuel* **2014**, *38*, 72–79. [[CrossRef](#)]
35. Mostafa, M.S.; Bakr, A.A.; Eshaq, G.; Kamel, M.M. Novel Co/Mo layered double hydroxide: Synthesis and uptake of Fe(II) from aqueous solutions (Part 1). *Desalin. Water Treat.* **2015**, *56*, 239–247. [[CrossRef](#)]
36. Deng, L.; Zeng, H.; Shi, Z.; Zhang, W.; Luo, J. Sodium dodecyl sulfate intercalated and acrylamide anchored layered double hydroxides: A multifunctional adsorbent for highly efficient removal of Congo red. *J. Colloid Interface Sci.* **2018**, *521*, 172–182. [[CrossRef](#)]
37. Cai, Y.; Huang, H.; Wang, L.; Zhang, X.; Yuan, Y.; Li, R.; Wan, H.; Guan, G. Facile synthesis of pure phase γ -AlOOH and γ -Al₂O₃ nanofibers in a recoverable ionic liquid via a low temperature route. *RSC Adv.* **2015**, *5*, 104884–104890. [[CrossRef](#)]
38. Bessaha, H.; Bouraada, M.; Demenoral, L.C. Removal of indigo carmine and green bezanyl-F2B from water using calcined and uncalcined Zn/Al + Fe layered double hydroxide. *J. Water Reuse. Desal.* **2017**, *7*, 152–161. [[CrossRef](#)]
39. Choi, J.-W.; Lee, S.-Y.; Park, K.-Y.; Lee, K.-B.; Kim, D.-J.; Lee, S.-H. Investigation of phosphorus removal from wastewater through ion exchange of mesostructure based on inorganic material. *Desalination* **2011**, *266*, 281–285. [[CrossRef](#)]
40. Brigante, M.; Schulz, P.C. Adsorption of paraquat on mesoporous silica modified with titania: Effects of pH, ionic strength and temperature. *J. Colloid Interface Sci.* **2011**, *363*, 355–361. [[CrossRef](#)]
41. Gad, H.M.H.; El-Sayed, A.A. Activated carbon from agricultural by-products for the removal of Rhodamine-B from aqueous solution. *J. Hazard. Mater.* **2009**, *168*, 1070–1081. [[CrossRef](#)] [[PubMed](#)]
42. Lagergren, S. About the theory of so called adsorption of soluble substances. *Handlingar* **1898**, *24*, 1–39.
43. Blanchard, G.; Maunay, M.; Martin, G. Removal of heavy metals from waters by means of natural zeolites. *Water Res.* **1984**, *18*, 1501–1507. [[CrossRef](#)]
44. Goscianska, J.; Ptazkowska-Koniarz, M.; Frankowski, M.; Franus, M.; Panek, R.; Franus, W. Removal of phosphate from water by lanthanum-modified zeolites obtained from fly ash. *J. Colloid Interface Sci.* **2018**, *513*, 72–81. [[CrossRef](#)] [[PubMed](#)]
45. Langmuir, I. The constitution and fundamental properties of solids and liquids Part I. Solids. *J. Am. Chem. Soc.* **1916**, *38*, 2221–2295. [[CrossRef](#)]
46. Hyder, A.H.M.G.; Begum, S.A.; Egiebor, N.O. Adsorption isotherm and kinetic studies of hexavalent chromium removal from aqueous solution onto bone char. *J. Environ. Chem. Eng.* **2015**, *3*, 1329–1336. [[CrossRef](#)]
47. Rodrigues, L.A.; da Silva, M.L.C.P. An investigation of phosphate adsorption from aqueous solution onto hydrous niobium oxide prepared by co-precipitation method. *Colloids Surf. A* **2009**, *334*, 191–196. [[CrossRef](#)]
48. Tran, N.; Drogui, P.; Blais, J.-F.; Mercier, G. Phosphorus removal from spiked municipal wastewater using either electrochemical coagulation or chemical coagulation as tertiary treatment. *Sep. Purif. Technol.* **2012**, *95*, 16–25. [[CrossRef](#)]
49. Freundlich, H. Über die adsorption in lösungen. *Zeitschrift für Physikalische Chemie* **1906**, *57*, 385–471. [[CrossRef](#)]

50. Dubinin, M.M.; Radushkevich, L.V. The equation of the characteristic curve of activated charcoal. *Proc. Acad. Sci. Phys. Chem. Sect.* **1947**, *55*, 327–329.
51. Kajjumba, G.W.; Yıldırım, E.; Aydın, S.; Emik, S.; Ağun, T.; Osra, F.; Wasswa, J. A facile polymerisation of magnetic coal to enhanced phosphate removal from solution. *J. Environ. Manag.* **2019**, *247*, 356–362. [[CrossRef](#)] [[PubMed](#)]
52. Tempkin, M.I.; Pyzhev, V. Kinetics of ammonia synthesis on promoted iron catalyst. *Acta Phys. Chim. USSR* **1940**, *12*, 327–356.
53. Basar, C.A. Applicability of the various adsorption models of three dyes adsorption onto activated carbon prepared waste apricot. *J. Hazard. Mater.* **2006**, *135*, 232–241. [[CrossRef](#)] [[PubMed](#)]
54. Staroń, P.; Chwastowski, J. Raphia-microorganism composite biosorbent for lead ion removal from aqueous solutions. *Materials* **2021**, *14*, 7482. [[CrossRef](#)]
55. Frumkin, A.N. A Multicomponent Isotherm for Gas Adsorption. *Z. Phys. Chem.* **1925**, *116*, 466–485. [[CrossRef](#)]
56. Harkins, W.D.; Jura, G. The decrease of free surface energy as a basis for the development of equations for adsorption isotherms; and the existence of two condensed phases in films on solids. *J. Chem. Phys.* **1944**, *12*, 112–113. [[CrossRef](#)]
57. Su, Y.; Cui, H.; Li, Q.; Gao, S.; Shang, J.K. Strong adsorption of phosphate by amorphous zirconium oxide nanoparticles. *Water Res.* **2013**, *47*, 5018–5026. [[CrossRef](#)]
58. Wu, Y.; Li, X.; Yang, Q.; Wang, D.; Xu, Q.; Yao, F.; Chen, F.; Tao, Z.; Huang, X. Hydrated lanthanum oxide-modified diatomite as highly efficient adsorbent for low-concentration phosphate removal from secondary effluents. *J. Environ. Manag.* **2019**, *231*, 370–379. [[CrossRef](#)]
59. Agarwal, S.; Tyagi, I.; Gupta, V.K.; Mashhadi, S.; Ghasemi, M. Kinetics and thermodynamics of malachite green dye removal from aqueous phase using iron nanoparticles loaded on ash. *J. Mol. Liq.* **2016**, *223*, 1340–1347. [[CrossRef](#)]
60. Fernandes, A.N.; Almeida, C.A.P.; Debacher, N.A.; Sierra, M.M.D.S. Isotherm and thermodynamic data of adsorption of methylene blue from aqueous solution onto peat. *J. Mol. Struct.* **2010**, *982*, 62–65. [[CrossRef](#)]
61. Seki, Y.; Yurdakoç, K. Adsorption of promethazine hydrochloride with KSF montmorillonite. *Adsorption* **2006**, *12*, 89–100. [[CrossRef](#)]
62. Mallakpour, S.; Tabesh, F. Tragacanth gum based hydrogel nanocomposites for the adsorption of methylene blue: Comparison of linear and non-linear forms of different adsorption isotherm and kinetics models. *Int. J. Biol. Macromol.* **2019**, *133*, 754–766. [[CrossRef](#)] [[PubMed](#)]
63. Melo, B.C.; Paulino, F.A.; Cardoso, V.A.; Pereira, A.G.; Fajardo, A.R.; Rodrigues, F.H. Cellulose nanowhiskers improve the methylene blue adsorption capacity of chitosan-g-poly(acrylic acid) hydrogel. *Carbohydr. Polym.* **2018**, *181*, 358–367. [[CrossRef](#)] [[PubMed](#)]